**Showcasing research from Professor Boris Mizaikoff's laboratory, Institute of Analytical and Bioanalytical Chemistry, Ulm University, 89081 Ulm, Germany.**

Infrared spectroscopy based on broadly tunable quantum cascade lasers and polycrystalline diamond waveguides

Recently emerging broadly tunable quantum cascade lasers (tQCL) emitting in the mid-infrared (MIR) are a versatile alternative to well established thermal emitters in combination with interferometers as applied in Fourier transform infrared (FTIR) spectroscopy. Combination of tQCLs with durable optical transducers, *i.e.* polycrystalline diamond as waveguide for attenuated total reflection (ATR) based spectroscopy opens possibilities to analyse the composition of biological and medical samples as complex as body fluids. The high-energy output of tQCLs in the MIR enables elongated optical path lengths, aka interaction path lengths with the potential to reliably detect minute analyte amounts.
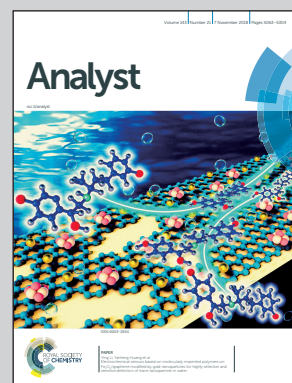
ROYAL SOCIETY OF **CHEMISTRY**

rsc.li/analyst

Check for updates

Infrared spectroscopy based on broadly tunable quantum cascade lasers and polycrystalline diamond waveguides

Julian Haas, [ID] [a,b] Ernesto Vargas Catalán,[b] Pierre Piron,[b] Mikael Karlsson*[b,c] and Boris Mizaikoff [ID] *[a]

Recently emerging broadly tunable quantum cascade lasers (tQCL) emitting in the mid-infrared (MIR) are a versatile alternative to well established thermal emitters in combination with interferometers as applied in Fourier transform infrared (FTIR) spectroscopy. The wide and highly spectrally resolved wavelength tuning characteristics along with superior spectral energy density renders laser-based vibrational spectroscopy methods an efficient alternative *vs.* conventional molecular spectroscopies. Using diamond in attenuated total reflection (ATR) sensing formats benefits from the physical robustness and chemical resistivity of the internal reflective element (IRE) material. While inherent material absorption frequently limits the optical path length within diamond ATR elements, the herein presented design combining bright tQCLs with a multi-reflection polycrystalline diamond (PCD) ATR element enables an optical beam path length of approximately 5 cm. Thereby, sensitive spectroscopic measurements in the MIR are enabled. As an example, non-invasive glucose monitoring in human saliva is examined, highlighting the potential benefits of the proposed analytical concept with regards to exquisite sensitivity and selectivity in combination with a robust sensing interface, *i.e.*, diamond. This approach paves the way towards directly analyzing molecular constituents in complex and potentially corrosive biomedical and biochemical matrices.

Introduction

Analysis in the mid-infrared (MIR) (2.5 μm to 25 μm, 4000 cm^{-1} to 400 cm^{-1}) is a spectroscopic strategy routinely deployed in a wide field of scenarios ranging from process analytics to biomedical applications.[1] However, limitations include the required relatively high analyte concentrations, rather high sample volumes in the mL range or above, and comparatively bulky instrument dimensions. Routinely used thermal emitters such as SiC globars provide a limited spectral energy density in the MIR, which directly relates to sensitivity limitations especially in strongly absorbing analyte matrices. However, recent progress in broadly tunable laser light source technology provides a promising alternative *vs.* established non-coherent light sources, as a significantly higher energy density per wavelength is intrinsically provided.

The introduction of quantum cascade lasers (QCLs) operating in the MIR has rendered this technology especially interest-

ing for (bio)chemical analysis and sensing tasks. Notably, two different approaches are being realized with QCL technology. On the one hand, high resolution can be achieved with distributed feed-back (DFB) technology, yet at the cost of narrower tuning ranges. On the other hand, external cavities (ECs) provide broader tuning ranges albeit at lower spectral resolution. Lately, QCL systems providing high resolution in combination with relatively broad tuning ranges (155 cm^{-1}) have been introduced using EC architectures.[2] Nowadays, QCL spectrometers are available providing tuning ranges up to 1100 cm^{-1} *via* up to four individual lasers[3–5] covering about 270 cm^{-1} each operated in parallel, and providing up to 500 mW of pulsed or continuous wave (CW) laser radiation. With increasing availability, QCL technology has already been used for detecting a variety of medical analytes.[6] For instance, the detection of trace amounts of cocaine has been demonstrated.[7,8]

Attenuated total reflection spectroscopy (ATR) makes use of an exponentially decaying evanescent field emerging at the surface of a waveguiding total internal reflection element (IRE) and is considered a complementary sampling strategy *vs.* transmission techniques. As an IRE or waveguide, high refractive index (RI, *n*) materials are required, which are ideally also chemically and physically resilient. Diamond combines these

[a]*Institute of Analytical and Bioanalytical Chemistry, Ulm University, Albert-Einstein-Allee 11, 89081 Ulm, Germany. E-mail: boris.mizaikoff@uni-ulm.de*
[b]*Department of Engineering Sciences, Uppsala University, Box 534, SE-75121 Uppsala, Sweden. E-mail: mikael.karlsson@angstrom.uu.se*
[c]*Molecular Fingerprint Sweden AB, Eksätravägen 130, SE-756 55 Uppsala, Sweden*

favorable properties and is therefore among the favored ATR element materials. However, single crystalline diamond (SCD) remains quite expensive to fabricate and process. In contrast, polycrystalline diamond (PCD) offers comparable performance in the MIR at approximately one tenth of the fabrication costs. Conventionally, the limited power output of standard MIR sources and the intrinsic optical absorption of diamond limits the propagation path length through diamond ATR elements, at which acceptable signal-to-noise ratios (SNR) can be achieved. This is the reason, why diamond ATR elements are predominantly configured as single internal reflection elements.

The reduction of bulk diamond crystal dimensions to thin-film waveguides and the introduction of more powerful MIR laser sources nowadays enables overcoming this limitation. Thin-film diamond waveguide technology in combination with laser sources has already been shown for the detection of organic compounds and proteins in the MIR.[9–11] In these contributions, free-standing core-only (i.e., air-clad) diamond thin-film waveguides supported by a silicon frame have demonstrated their utility for analytical applications. However, processing limitations including high strain within the deposited diamond layers, thermal expansion, and demanding processing parameters at elevated temperatures in a hydrogen atmosphere compete with matching the required optical parameters such as the refractive index. Thin-film diamond growth on silicon substrates with subsequent partial removal of the supporting substrate is a tradeoff between stable growth conditions and refractive index matching at the expense of potentially more elaborate processing opportunities for waveguide fabrication. Although free-standing diamond structures are self-supporting, they remain brittle in nature and are therefore mechanically sensitive, which is not an issue for bulk diamond IREs.

The physical and chemical resistivity, biocompatibility, and autoclavability of diamond renders analytical concepts based on diamond ideally suited for bioanalytics. Body fluids are a rich and well-known source of biomarkers relevant in medical diagnostics and for clinical monitoring. In particular, non-invasive alternatives to blood or spinal fluid are more convenient for patients and less prone to potential complications such as inflammation due to the puncture. Even tear fluid, sweat or urine samples are inconvenient to obtain. With globally increasing diabetic rates, non-invasive glucose testing is of increasing interest, and has become a driving force in the development of non-invasive analytical devices.[12,13] Exemplarily, non-invasive blood glucose monitoring has been presented by the research group of Mäntele utilizing QCLs and photoacoustic cells. Detection of <50 mg dL^{-1} up to >300 mg dL^{-1}, which is in the clinically relevant regime has been achieved.[14,15] Furthermore, non-invasive electrochemical determination of glucose in human saliva has been presented.[16] In general, saliva appears to be a readily obtainable human body fluid suitable for medical diagnostics,[17] comparable to expired human breath.[18] Exhaled breath analysis has matured into a frequently applied strategy to obtain CO_2 and

volatile organic compound (VOC) concentrations, while saliva comprises a certain percentage of condensed breath constituents. Furthermore, buccal spectral markers have been found to correlate to potential lung cancer risks.[19] Even the detection of α-synuclein serving as a potential biomarker for Parkinson's disease in cheek cell samples has been shown.[20] Likewise, simple molecules such as salivary uric acid are non-invasively addressable biomarkers for metabolic syndrome.[21,22] Even physiological stress has been shown to correlate with changes in the salivary composition, and the associated MIR spectral features.[23] Infrared spectroscopy has also been applied to detect protein shifts of psoriatic and diabetic patients in saliva.[24] Notwithstanding, a potential spectral correlation between blood glucose and salivary glucose has been proposed in literature.[25,26] Biologically relevant concentrations of glucose in saliva are reported to range from 0.008 mg mL^{-1} to 0.0105 mg mL^{-1} (ref. 16 and 27) in healthy patients, and from 0.04 mg mL^{-1} to 0.14 mg mL^{-1} for diabetic patients.[26] This is approximately one tenth of the concentration range expected in blood extending from 0.88 mg mL^{-1} to 0.94 mg mL^{-1}.[28] Hence, improved sensitivities especially for IR sensing schemes are required for glucose analysis in saliva.

In the present study, an IR spectroscopic analysis system based on a tQCL in combination with a PCD IRE has been developed. The utility of the system for addressing the MIR fingerprint regime enabling non-invasive saliva glucose level analysis is evaluated.

Experimental method: MIR evanescent field sensing system based on a PCD optical transducer

Saliva sampling

Approx. 1 mL of saliva was sampled from a healthy volunteer, between 20 and 30 years old (BMI 26.7) per trail by unstimulated drooling. Prior to sampling, no food or beverages were allowed for one hour to avoid interference of residual food remains in the oral cavity such as proteins, fat or hydrocarbons with the subsequent analysis. Directly before sampling, present saliva was swallowed and the oral cavity was rinsed with approx. 50 mL of mineral water ensuring recently produced saliva. For time-dependent analyses, samples were collected every 10 min.

The saliva samples were obtained according to the Declaration of Helsinki.[29] The healthy volunteer was instructed orally and by writing and has given written consent.

Experimental QCL setup

The experimental setup (Fig. 1) is based on a broadly tunable mid infrared quantum cascade laser system (MIRcat, Daylight Solutions). The laser head comprises of four individual broadly tunable quantum cascade lasers, optically coupled into one single output port. Thus, a spectral range coverage from 4.95 μm to 11.2 μm (2020 cm^{-1} to 890 cm^{-1}) is provided at a peak output power (i.e., at the center wavelength of each
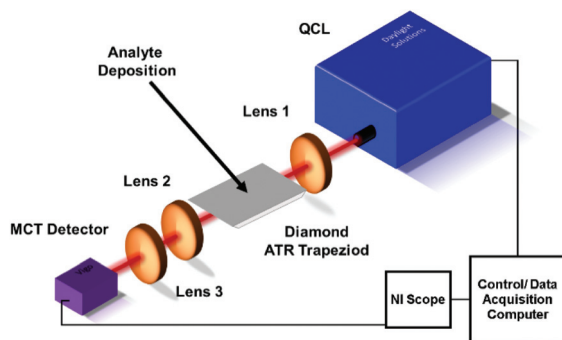
Fig. 1 Schematic of the experimental QCL PCD ATR IRE setup. Apertures between QCL and lens 1, and between lens 2 and 3 are not shown for clarity.

Fig. 2 Trajectories of IR rays within the diamond ATR trapezoid visualized *via* ray tracing.

parabolic emission curve of the particular laser) of approx. 500 mW. The lasers were operated in pulsed mode at a pulse width of 400 ns, and at a repetition rate of 100 kHz. The laser head was thermoelectrically cooled (TEC) to 17 °C. The laser head emitted 100 : 1 vertically polarized radiation in a collimated beam. The emitted beam was focused with a ZnSe lens (Thorlabs, aspheric, focal length 25 mm) onto the incoupling facet of the diamond trapezoid. The diamond trapezoid had beveled in- and out-coupling facets with an angle of 45° ensuring optimized total internal reflection within the diamond crystal. The beveled facets were cut and polished at the desired trapezoidal shape. The polycrystalline diamond IRE was grown *via* chemical vapor deposition (CVD) by Diamond Materials (Diamond Materials GmbH, Freiburg, Germany). Radiation emanating at the distal end of the diamond IRE was collected with a second ZnSe lens (Thorlabs, aspheric, focal length 25 mm), and focused onto a detector *via* a third ZnSe lens (Thorlabs, aspheric, focal length 12.7 mm). Additional apertures between the laser and the first lens, and between the second and third lens allowed further beam shaping and intensity control. The detector (PVMI-4TE 12 PIP-PC 200-M-F-M4, Vigo Systems S. A., Poland) was based on a TEC MCT (mercury cadmium telluride) detector crystal optically immersed into a GaAs (gallium arsenide) hypersphere, which is optimized for detection at a wavelength of 10.6 μm. Data acquisition was performed with a National Instrument PC oscilloscope (NI PXIe-5114 125 MHz, 250 MS/s, 8-bit. Oscilloscope; NI PXIe 1071case; NI PXIe-8360 express card), which was operated *via* a LabView (LabView 2016) script. The script was based on tuning the QCL emission wavelength in 1 cm^{-1} increments. For each spectrum, a single channel background spectrum (I_0) and a single channel sample spectrum (I) were recorded across the entire tuning range of the laser system, and absorbance (A) spectra were calculated as $A = -\log_{10}(I/I_0)$.

Results and discussion

Evaluation of the optical properties

The utilized PCD with a surface area of 15 × 12 mm^2 with beveled in- and out-coupling facets at an angle of 45° and a
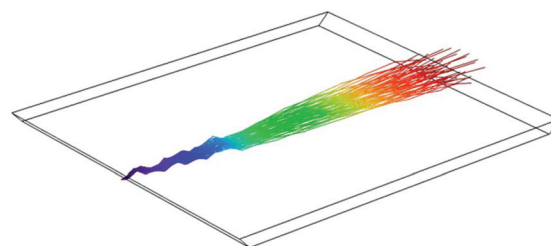
thickness 450 ± 50 μm was modeled *via* ray tracing in COMSOL Multiphysics (Version 5.2a, COMSOL Multiphysics GmbH) to evaluate the waveguiding properties of the diamond trapezoid. Using geometrical ray tracing considerations, considering an ideal focused beam with 20 μm diameter, on an average, 17 reflections with 8 reflections accessible at the top IRE surface and approx. 4.8 cm propagation path length were calculated along the length of the diamond trapezoid. Furthermore, focusing IR radiation onto the beveled in-coupling facet enabled internal reflections at angles steeper than the critical angle $\theta_{crit} = 25°$ (θ_{crit} = arcsine ($n_{Air}/n_{Diamond}$) = arcsine (1/2.4)) *vs.* the surface normal *via* self-defocusing of the radiation within the diamond crystal (Fig. 2).

PCD characterization

The spectral characteristics of PCD in the MIR were evaluated using an IFS 66 v/s FTIR spectrometer, and were compared to a SCD specimen of the same thickness (approx. 450 μm). The spectrometer was equipped with a room-temperature DTGS (deuterated L-alanine glycine sulfate) detector (Bruker Optik GmbH). Data was recorded *via* the OPUS software package (Build 6.5, Bruker Optik GmbH) at a spectral resolution of 4 cm^{-1} in the range of 4000–600 cm^{-1} (2.5–16.7 μm) averaging 32 scans for each spectrum. The diamond samples were mounted within a transmission holder in order to propagate the IR beam through the 450 μm thick material, *i.e.* perpendicular to the beam direction used for QCL ATR measurements. Finally, data was evaluated *via* Origin (OriginPro 2017G, OriginLab). As shown in Fig. 3, no significant difference between SCD and PCD diamond in grain growth direction was apparent. While weak Rayleigh scattering may still occur, it should be negligible towards longer wavelengths following ~$1/\lambda^4$ within the crystal boundaries of the IRE.[30,31] Furthermore, interference with sp^2 hybridized graphitic carbon at crystallite boundaries appears negligible. It should be noted that non-sp^3 hybridized carbon atoms within the first few deposited PCD layers have been removed by polishing. Inherent diamond lattice vibrations (*i.e.*, two-phonon absorptions) are however present, and render IR studies in the spectral region of 2600–1500 cm^{-1} of limited utility due to the reduced energy throughput.
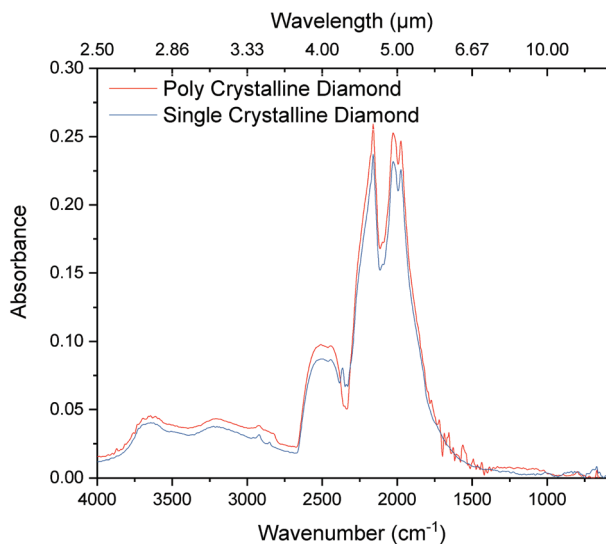
Fig. 3 PCD *versus* SCD revealing inherent two-phonon absorptions in the range 2600–1500 cm^{-1}. The MIR spectral fingerprint region ranging from approx. 1800–800 cm^{-1} is ideally suited for evanescent field absorption studies and shows similar transparence for SCD and PCD.

Using a QCL light source, higher spectral energy density is achieved, which renders the spectral regions close to the two-phonon absorption features still useful for analytical applications. As shown in Fig. 4, parabolic emission curves of the four applied laser crystals with intensity maxima around 1900 cm^{-1}, 1600 cm^{-1}, 1350 cm^{-1}, and 1100 cm^{-1} (5.25 μm, 6.25 μm, 7.5 μm, and 9 μm, respectively), are superimposed by the diamond lattice absorption emerging towards the shorter wavelength regime. Notably, transmission is still
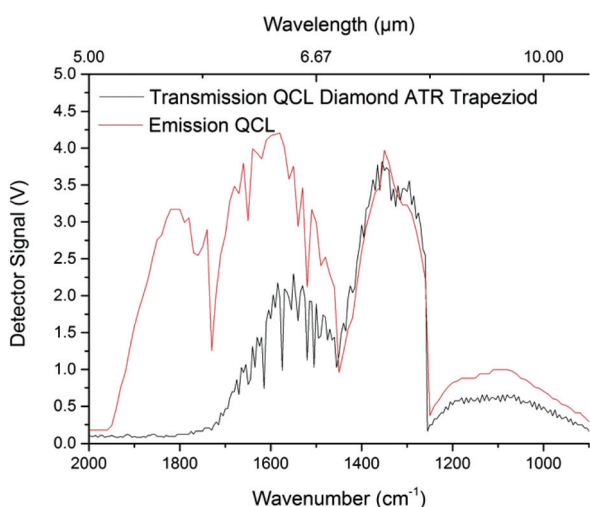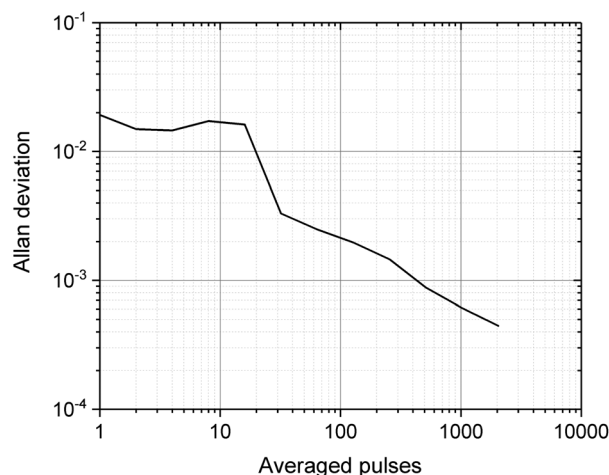
achieved up to 1800 cm^{-1} although IR radiation has already been propagated approx. 5 cm through the trapezoid PCD IRE structure.

Optimization of the laser light source

Due to pulsed operation of the QCLs, intensity deviations in between subsequent pulses had to be efficiently suppressed, which is commonly achieved by averaging a sufficient number of subsequent pulses. Using an Allan deviation experiment, the most suitable number of averaged laser pulses has been determined.[32–34] Resulting, 10 000 subsequent laser pulses were recorded, and their Allan variance has been plotted (Fig. 5). Consequently, 500 subsequent pulses were averaged during all further experiments as a trade-off between noise reduction (*i.e.*, Allan deviation <10^{-3}), and adequately short measurement times. Furthermore, 5-point adjacent-point-averaging was performed on the retrieved spectra to reduce inter-wavelength intensity deviations arising from the step-wise tuning of the lasers.

Analysis of human saliva

Human saliva analysis was selected as an application example due to its accessibility, while constituting a real-world complex biological matrix.[35] In human saliva, various organic molecules are present resulting in distinct fingerprint absorption bands in the MIR, *i.e.*, hydrocarbons, fats (~1100 cm^{-1}), and proteins, *i.e.*, around 1650 cm^{-1} assigned to the C=O stretching mode (amide I band), and around 1550 cm^{-1} assigned to a N–H bending mode (amide II band). Furthermore, symmetric and asymmetric stretching mode bands of carboxylate (COO^{-}) are present around 1400 cm^{-1} (Fig. 6). The latter can be assigned to lactic acid molecules or protein side chains with changes evident when comparing diabetic and non-diabetic patients. In an exemplary study, glucose levels in a healthy volunteer were evaluated. A distinct band at 1030 cm^{-1} was

Fig. 4 Emission of the four individual QCLs coupled into a single IR beam (red line). Single channel transmission through the PCD ATR trapezoid using this QCL assembly reveals the emission characteristics of the individual QCLs, superimposed by the two-phonon absorptions of diamond at wavelengths <5.56 μm (1800 cm^{-1}) (black line).

Fig. 5 Allan deviation/variance for an emission wavelength of 6 μm (1666 cm^{-1}). Adequate Allan deviation is reached after averaging 500 pulses *vs.* acceptable measurement times.
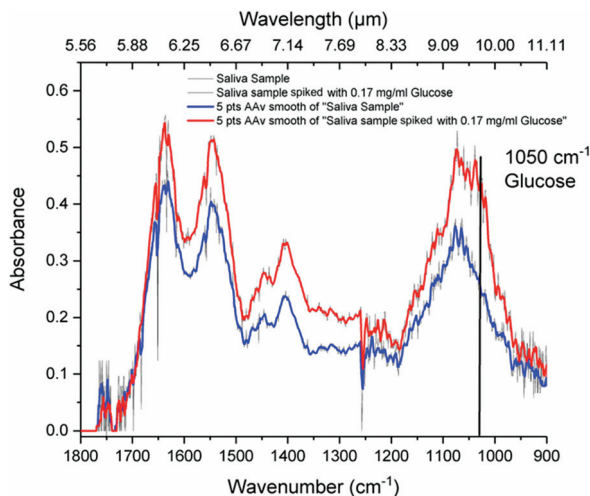
Fig. 6 Saliva spectra after evaporation of the volatile components, *i.e.*, mainly the water matrix. Protein bands (~1650 cm^{-1}, C=O stretching, amide I; ~1550 cm^{-1} N–H bending, amide II band), carboxylate bands (~1400 cm^{-1}, v_sCOO$^-$ and v_{as}COO$^-$ stretching vibrations), fat, and hydrocarbon bands (~1100 cm^{-1}) are evident. The band at 1030 cm^{-1} is associated with glucose and has been highlighted accordingly.


Fig. 7 Processed spectra for peak deconvolution (grey) along with fitted Lorentz peaks (colored). (a) Raw saliva sample. (b) Saliva sample spiked with 0.17 mg mL^{-1} glucose.

selected for the glucose determination within the MIR spectrum of saliva, which represents the CO vibrations of the glucose molecule.[36]

Per analysis, the obtained saliva samples were divided into equal aliquots, and spiked with aqueous solutions of alpha(+) D-glucose (M = 180.16 g mol^{-1}, VWR International GmbH) for establishing calibration samples *via* standard addition. Subsequently, 20 µL of each solution were transferred with an Eppendorf Pipette onto the PCD ATR IRE and the aqueous matrix was left to evaporate. A volume of 20 µL was determined to cover the surface of the diamond crystal, while avoiding spills affecting the in- and outcoupling facets. However, introducing an appropriately sealed liquid cell is supposed to enhance the reproducibility during future experiments by reducing variances resulting from viscosity variations of the saliva sample.

After each analysis, the crystal was cleaned with water, acetone, and isopropanol/lens cleaning tissue, which effectively removed the previous sample. The spectral region of interest within the obtained spectra for glucose determination was limited to 1200–900 cm^{-1}. The spectral region was smoothed with a 0.02 Hz low pass FFT filter, and subsequently normalized. In a next step, peak deconvolution was performed using Lorentz shaped bands fitted to the spectra. The peak centered at 1030 cm^{-1} characteristic for glucose was then integrated for quantification. An exemplary peak fit is shown in Fig. 7 for an unspiked sample, and for a sample spiked with 0.17 mg mL^{-1} glucose.

With the developed experimental procedure, a limit of detection (LOD) of 0.02 mg mL^{-1} (0.12 mmol L^{-1}) was derived using the 3σ noise criterion. This LOD is close to biologically relevant concentrations derived from literature for
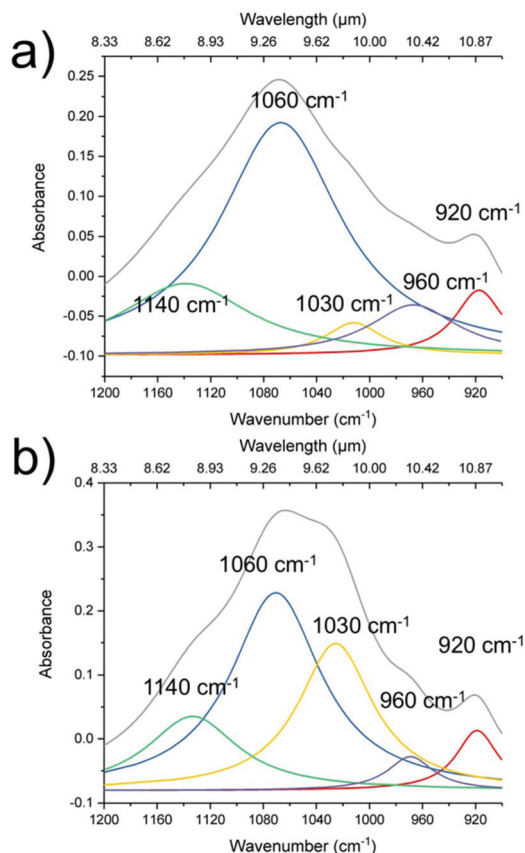
saliva ranging from 0.008 mg mL^{-1} to 0.0105 mg mL^{-1} (ref. 16) for baseline values of healthy patients, and is well below the expected values for analyzing saliva glucose levels in diabetic patients ranging from 0.04 mg mL^{-1} to 0.14 mg mL^{-1}.[26]

Time-dependent variation of saliva glucose levels was evaluated on a healthy volunteer between 20 and 30 years old (BMI 26.7). After one hour of base line monitoring, 500 mL of regular Coca Cola (Coca Cola Company) were consumed to deliberately rise saliva sugar levels (*i.e.*, 10.6 g of carbohydrates – mainly sucrose – per 100 mL).

Fig. 8 shows the time-dependent development of saliva glucose levels. Within the first 60 min, the saliva glucose level shows a variance between 0.05 mmol L^{-1} (0.01 mg mL^{-1}) and 0.35 mmol (0.06 mg mL^{-1}) around an average of about 0.2 mmol L^{-1} (0.04 mg mL^{-1}). This elevated variance is explained by variations of the saliva production itself and potential manual sample handling issues and have to be further substantiated during future studies. For example, inter-sample variances may be addressed by the addition of an internal standard. Deviations in saliva flow, resulting amount of saliva, and viscosity, as well as tissue or gland aspects may be addressed as well using this procedure. A slight decrease of
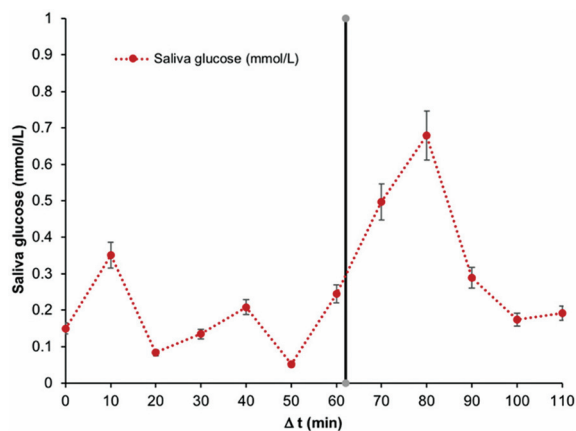
Fig. 8 Time-dependent saliva glucose monitoring. The black bar represents the time of intake of 500 mL of a carbohydrate-rich beverage. Saliva glucose levels in mmol L^{-1} are plotted for a time period of 110 min.

the glucose level after 30 min can be explained with an increased amount of time since the last meal. After intake of 500 mL of a sugary beverage within about one minute, 60 min after starting the experiment, an increase of salivary glucose levels is apparent. Careful rinsing of the oral cavity was of particular importance at this point to ensure that fresh saliva is evaluated rather than a mixture of the consumed beverage and saliva. The salivary glucose levels revealed a similar increase up to 0.7 mmol L^{-1} (0.13 mg mL^{-1}), yet dropped after a short period of time, *i.e.*, already after 40 min back to the baseline level of 0.2 mmol L^{-1} (0.04 mg mL^{-1}). Interference of beverage residues can be excluded, since the salivary glucose peak concentration is reached just after 20 min, while residual beverage should interfere already at an earlier stage.

While the exemplary analysis of glucose in saliva herein has been selected as an example demonstrating the device performance for analysis in a complex real-world matrix, further research on improved evaluation algorithms and with an increased number of patients has to be executed for evaluating the potential relationship between blood and glucose levels.[37]

For a more precise and accurate quantitative evaluation of salivary glucose levels, the complexity of the molecular composition of saliva requires applying advanced multivariate calibration algorithms during further studies to adequately represent potentially interfering molecules such as glycated proteins, inorganic salts, *etc*.

Conclusions and outlook

The combination of a broadly tunable QCL assembly serving as a bright mid-infrared light source in combination with polycrystalline diamond ATR IRE has been shown. The latest generation of tQCLs provides high spectral energy density across a broad and customizable spectral window, as required for target-specific device design or broadband analyte detection.

The developed PCD IRE element was ideally suited as a robust multi-reflection ATR IRE and sampling interface, which may be further optimized in dimensions according to the sensitivity demands of the respective applications to meet possible future handheld solutions due to the inherent possibility for size reduction of the presented system. Micro-chip sized tQCLs in combination with an IRE that is reduced to thin-film waveguide dimensions are potentially promising candidates for future personal health care applications that can be developed based on the presented results. The utility of this system for analysis of saliva glucose levels has been exemplarily shown. The achieved limit of detection (0.02 mg mL^{-1}) is well within the required range for evaluating medical samples. Clearly, a broader applicability of the presented concept has to be further evaluated analyzing saliva samples of large cohorts of diabetic *vs.* non-diabetic patients, and further validated using approved glucose analysis strategies along with multivariate statistical data analysis strategies for improved interpretation *vs.* interfering spectral features since correlation of salivary and blood glucose levels is highly controversial and challenging.[38] Furthermore, the detection of additional biomarkers of medical significance or the investigation of demanding (*e.g.*, corrosive) analyte media appears feasible due to the resilience and robustness of a PCD waveguide. In a next step, surface chemistries will be applied towards further signal enhancement capitalizing on chem/bio sensing strategies.[39] It is anticipated that covalent as well as non-covalent binding strategies enable the immobilization of molecular recognition or signal enhancing motifs, and the targeted accumulation/enrichment of selected molecules within the evanescent field.[40–42] Last but not least, PCD waveguides not only expand the application horizon of MIR spectroscopy, but even enable the inherent introduction of complementary analysis techniques such as spectro-electrochemistry *via* boron-doping of the PCD material.[43]

Author contributions

All authors have given approval to the final version of the manuscript.

Conflicts of interest

The authors declare no competing financial interest.

Acknowledgements

Notes and references

1 J. Haas and B. Mizaikoff, *Annu. Rev. Anal. Chem.*, 2016, **9**, 45–68.

2 G. Wysocki, R. Lewicki, R. F. Curl, F. K. Tittel, L. Diehl, F. Capasso, M. Troccoli, G. Hofler, D. Bour, S. Corzine, R. Maulini, M. Giovannini and J. Faist, *Appl. Phys. B*, 2008, **92**, 305–311.

3 M. Grafen, K. Nalpantidis, D. Ihrig, H. M. Heise and A. Ostendorf, *Proc. SPIE*, 2016, **9715**, 971517.

4 M. Grafen, K. Nalpantidis, A. Ostendorf, D. Ihrig and H. M. Heise, *Proc. SPIE*, 2016, **9715**, 97150T.

5 T. Vahlsing, H. Moser, M. Grafen, K. Nalpantidis, M. Brandstetter, H. M. Heise, B. Lendl, S. Leonhardt, D. Ihrig and A. Ostendorf, *Proc. SPIE-OSA*, 2015, **9537**, 953713.

6 A. Schwaighofer, M. Brandstetter and B. Lendl, *Chem. Soc. Rev.*, 2017, **46**, 5903–5924.

7 Y.-C. Chang, P. Wägli, V. Paeder, A. Homsy, L. Hvozdara, P. van der Wal, J. Di Francesco, N. F. de Rooij and H. Peter Herzig, *Lab Chip*, 2012, **12**, 3020.

8 P. Wägli, Y. C. Chang, A. Homsy, L. Hvozdara, H. P. Herzig and N. F. De Rooij, *Anal. Chem.*, 2013, **85**, 7558–7565.

9 X. Wang, M. Karlsson, P. Forsberg, M. Sieger, F. Nikolajeff, L. Österlund and B. Mizaikoff, *Anal. Chem.*, 2014, **86**, 8136–8141.

10 Á. I. López-Lorente, P. Wang, M. Sieger, E. Vargas Catalan, M. Karlsson, F. Nikolajeff, L. Österlund and B. Mizaikoff, *Phys. status solidi*, 2016, **213**, 2117–2123.

11 M. Malmström, M. Karlsson, P. Forsberg, Y. Cai, F. Nikolajeff and F. Laurell, *Opt. Mater. Express*, 2016, **6**, 1286.

12 R. Poddar, J. T. Andrews, P. Shukla and P. Sen, 2008, arXiv:0810.5755 [physics.med-ph], pp. 1–47.

13 A. Soni and S. K. Jha, *Biosens. Bioelectron.*, 2015, **67**, 763–768.

14 M. A. Pleitez, T. Lieblein, A. Bauer, O. Hertzberg, H. von Lilienfeld-Toal and W. Mäntele, *Anal. Chem.*, 2013, **85**, 1013–1020.

15 M. A. Pleitez, T. Lieblein, A. Bauer, O. Hertzberg, H. von Lilienfeld-Toal and W. Mäntele, *Rev. Sci. Instrum.*, 2013, **84**, 084901.

16 W. Zhang, Y. Du and M. L. Wang, *Sens. Bio-Sensing Res.*, 2015, **4**, 23–29.

17 B. Michalke, B. Rossbach, T. Göen, A. Schäferhenrich and G. Scherer, *Int. Arch. Occup. Environ. Health*, 2014, **88**, 1–44.

18 T. Mathew, P. Pownraj, S. Abdulla and B. Pullithadathil, *Diagnostics*, 2015, **5**, 27–60.

19 A. J. Radosevich, N. N. Mutyal, J. D. Rogers, B. Gould, T. A. Hensing, D. Ray, V. Backman and H. K. Roy, *PLoS One*, 2014, **9**, e110157.

20 T. Stewart, Y.-T. Sui, L. F. Gonzalez-Cuyar, D. T. W. Wong, D. M. Akin, V. Tumas, J. Aasly, E. Ashmore, P. Aro, C. Ginghina, A. Korff, C. P. Zabetian, J. B. Leverenz, M. Shi and J. Zhang, *Neurobiol. Aging*, 2014, **35**, 418–420.

21 M. Soukup, I. Biesiada, A. Henderson, B. Idowu, D. Rodeback, L. Ridpath, E. G. Bridges, A. M. Nazar and K. Bridges, *Diabetol. Metab. Syndr.*, 2012, **4**, 14.

22 L. A. Soares Nunes, S. Mussavira and O. Sukumaran Bindhu, *Biochem. Med.*, 2015, **25**, 177–192.

23 P. C. Caetano Júnior, J. F. Strixino and L. Raniero, *Res. Biomed. Eng.*, 2015, **31**, 116–124.

24 U. Bottoni, R. Tiriolo, S. A. Pullano, S. Dastoli, G. F. Amoruso, S. P. Nistico and A. S. Fiorillo, *IEEE Trans. Biomed. Eng.*, 2016, **63**, 379–384.

25 D. A. Scott, D. E. Renaud, S. Krishnasamy, P. Meriç, N. Buduneli, Ş. Çetinkalp and K.-Z. Liu, *Diabetol. Metab. Syndr.*, 2010, **2**, 48.

26 S. Kumar, S. Padmashree and R. Jayalekshmi, *Contemp. Clin. Dent.*, 2014, **5**, 312.

27 A. Borg and D. Birkhed, *Scand. J. Dent. Res.*, 1988, **96**, 551–556.

28 M. Brandstetter, L. Volgger, A. Genner, C. Jungbauer and B. Lendl, *Appl. Phys. B*, 2013, **110**, 233–239.

29 World Medical Association, *J. Am. Med. Assoc.*, 2013, **310**, 2191.

30 A. J. Cox, A. J. DeWeerd and J. Linden, *Am. J. Phys.*, 2002, **70**, 620–625.

31 J. E. Graebner, M. E. Reiss, L. Seibles, T. M. Hartnett, R. P. Miller and C. J. Robinson, *Phys. Rev. B*, 1994, **50**, 3702–3713.

32 P. Werle, *Appl. Phys. B*, 2011, **102**, 313–329.

33 P. Werle, R. Muecke and F. Slemr, *Appl. Phys. B: Photophys. Laser Chem.*, 1993, **57**, 131–139.

34 I. José Gomes da Silva, E. Tütüncü, M. Nägele, P. Fuchs, M. Fischer, I. M. Raimundo and B. Mizaikoff, *Analyst*, 2016, **141**, 4432–4437.

35 P. D. V. de Almeida, A. M. T. Grégio, M. A. N. Machado, A. A. S. de Lima and L. R. Azevedo, *J. Contemp. Dent. Pract.*, 2008, **9**, 72–80.

36 S. Kino, S. Omori, T. Katagiri and Y. Matsuura, *Biomed. Opt. Express*, 2016, **7**, 701.

37 C. Naing and J. W. Mak, *J. Diabetes Metab. Disord.*, 2017, **16**, 2.

38 M. Grafen, S. Delbeck, H. Busch, H. M. Heise and A. Ostendorf, in *Optical Diagnostics and Sensing XVIII: Toward Point-of-Care Diagnostics*, ed. G. L. Coté, SPIE, 2018, p. 9.

39 A. Krueger and D. Lang, *Adv. Funct. Mater.*, 2012, **22**, 890–906.

40 V. Vermeeren, S. Wenmackers, P. Wagner and L. Michiels, *Sensors*, 2009, **9**, 5600–5636.

41 P. O. Andersson, P. Viberg, P. Forsberg, F. Nikolajeff, L. Österlund and M. Karlsson, *Anal. Bioanal. Chem.*, 2016, **408**, 3675–3680.

42 T. Nakamura, T. Ohana and M. Hasegawa, *New Diamond Front. Carbon Technol.*, 2005, **15**, 313–324.

43 K. Bennet, K. Lee, J. Kruchowski, S.-Y. Chang, M. Marsh, A. Van Orsow, A. Paez and F. Manciu, *Materials*, 2013, **6**, 5726–5741.